Three-dimensional MHD simulation of solar wind using a new boundary treatment: Comparison with in-situ data at Earth

Fang Shen[1,2], Zicai Yang[1], Jie Zhang[3] and Xueshang Feng[1,2]

[1]SIGMA Weather Group, State Key Laboratory of Space Weather, NSSC, CAS, Beijing, China

[2]HIT Institute of Space Science and Applied Technology, Shenzhen, China

[3]Department of Physics and Astronomy, George Mason University, Fairfax, VA 22030, USA

2018-09-26, WG3, ISEST 2018,
Hvar, Croatia

Outline:

- Introduction
- MHD Model
- New Boundary Treatment
- Simulation Results
- Discussion and Summary

Solar Wind Prediction Models:

- Full empirical Model
- Hybrid empirical/physics-based Model
- Full physics-based Model

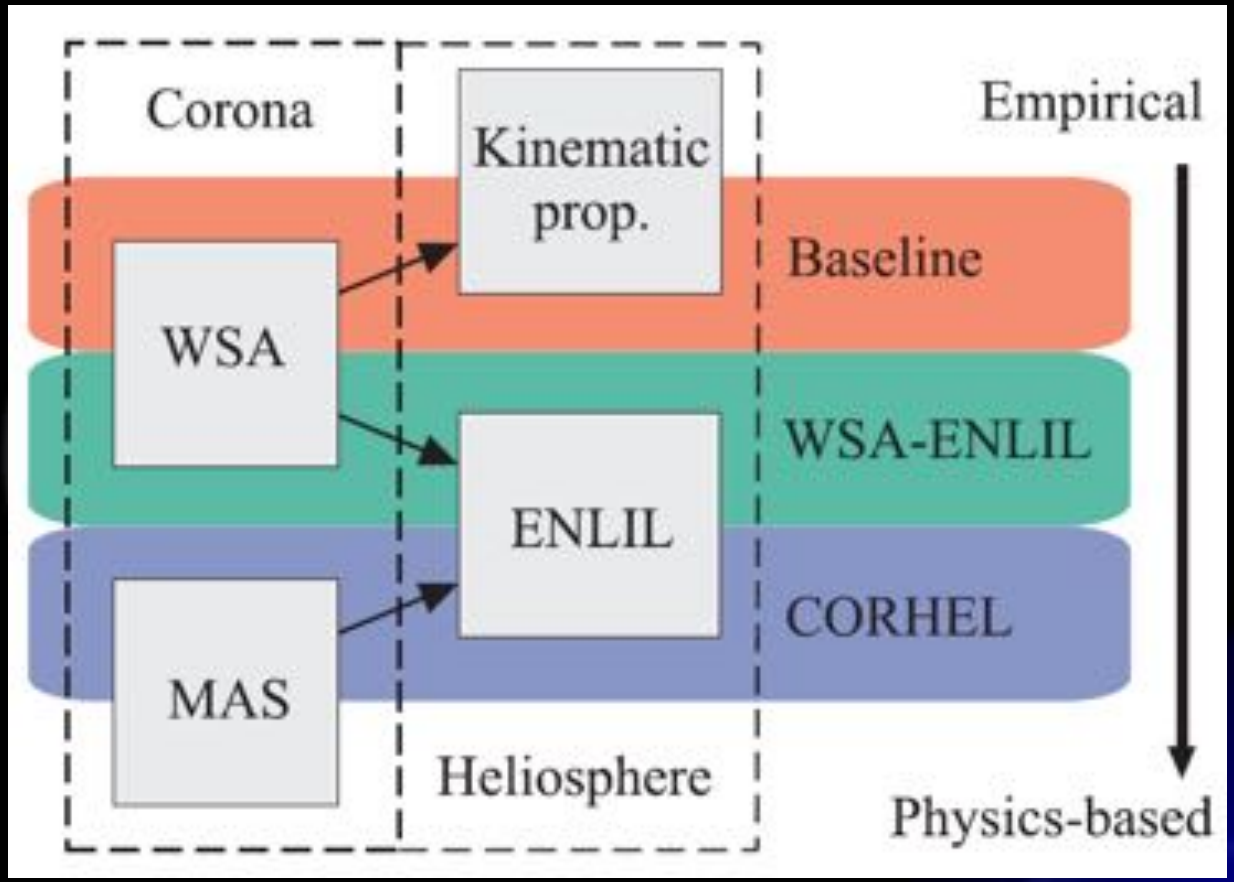

(Owen et al., 2008, *Space Weather*)

SIGMA WEATHER GROUP

(Gressl et al., 2014, *Sol. Phys.*)

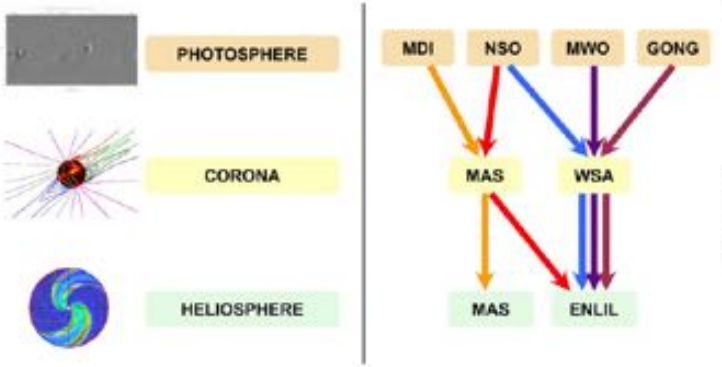

Predictive Science, Inc.

Community Coordinated Modeling Center

MAS/MAS (MDI)

MAS/ENLIL (NSO)

WSA/ENLIL (NSO)

WSA/ENLIL (MWO)

WSA/ENLIL (GONG)

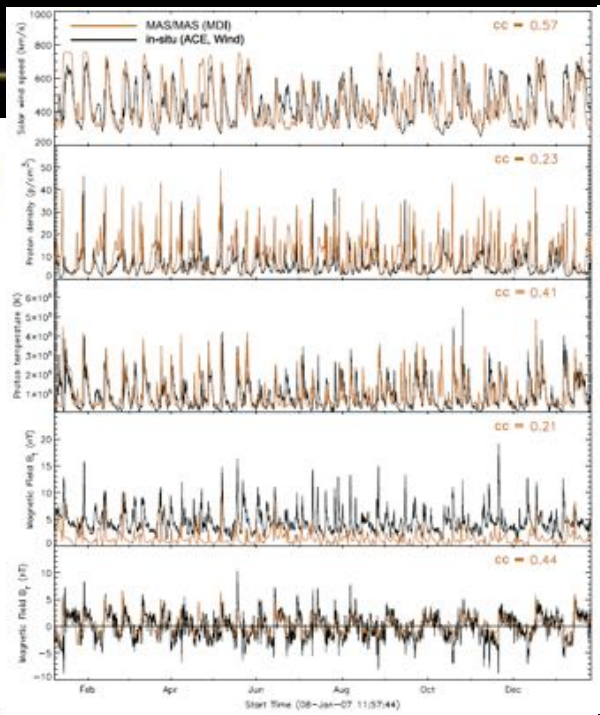

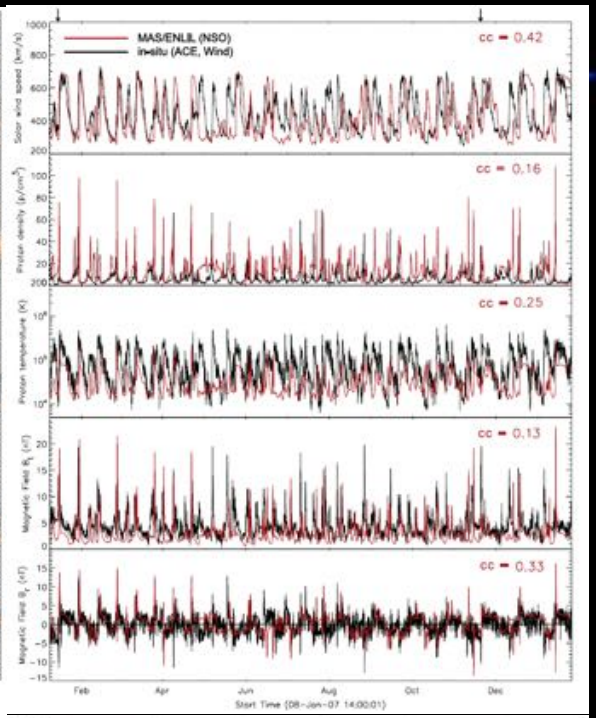

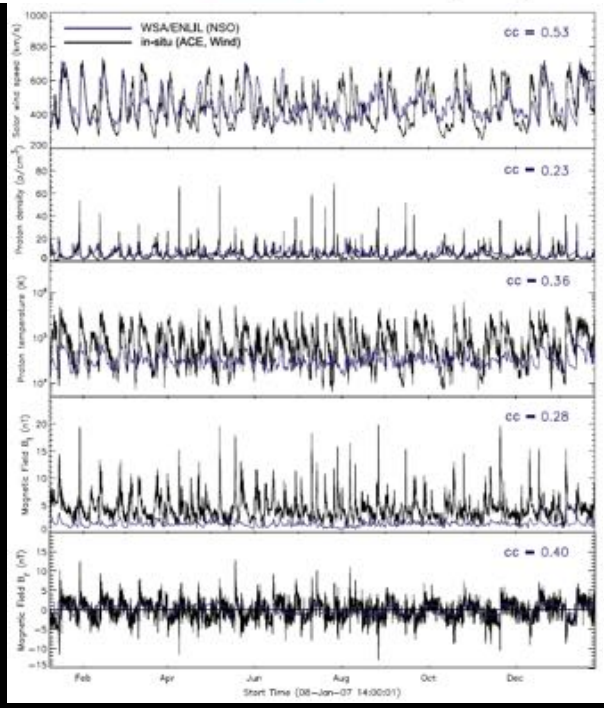

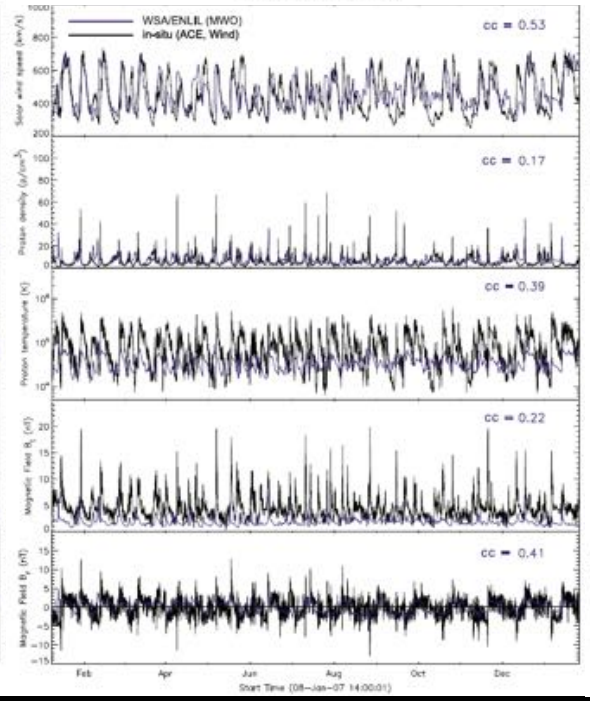

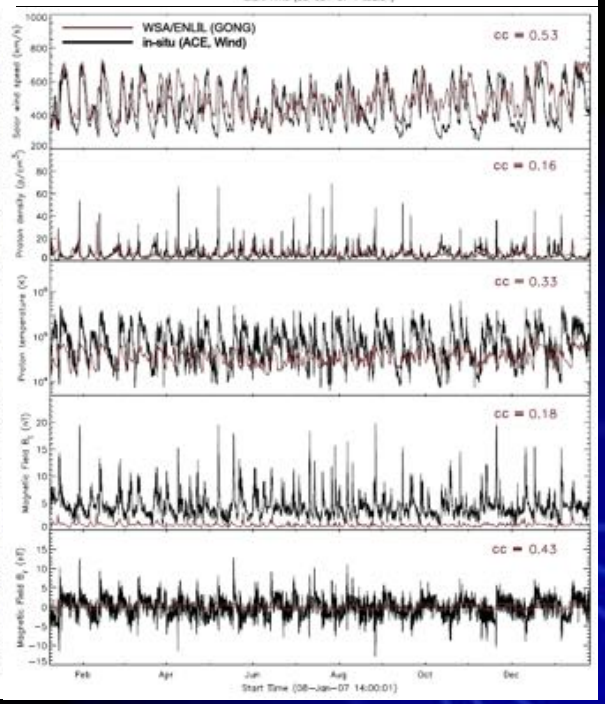

- The hybrid empirical/physics-based models are comparable with the full physics-based models in reproducing the large-scale structure of the solar wind. Therefore, with respect to time-efficiency and prediction accuracy, the hybrid models remain an important tool in the prediction of solar wind parameters in the near future;
- The treatment of the lower boundary condition plays a crucial role in the hybrid models, especially in influencing the consistency between the simulation results and the observations over the long term, *e.g.*, over solar cycles.
- In this presentation, based on our previous 3D COIN-TVD MHD model [e.g., Feng et al., 2003, 2005; Shen et al., 2007, 2009, 2011, 2012, 2013, 2014], we propose and implement a new method of treating the boundary condition, which is the base of establishing a hybrid empirical and 3D heliospheric MHD model, so as to simulate the solar wind for different phases of solar cycle.

MHD Equations

- $\frac{\partial \rho}{\partial t} + \nabla \cdot (\rho \boldsymbol{V}) = 0$ (1)

$$\frac{\partial \rho \boldsymbol{V}}{\partial t} + \nabla \cdot \left[\left(p + \frac{B^2}{2\mu_0}\right)\boldsymbol{I} + \rho \boldsymbol{V}\boldsymbol{V} - \frac{\boldsymbol{B}\boldsymbol{B}}{\mu_0}\right] = -\frac{\rho G M_s}{r^3}\boldsymbol{r} + \boldsymbol{V} \cdot \boldsymbol{f} \quad (2)$$

$$\frac{\partial B}{\partial t} + \nabla \cdot (\boldsymbol{V}\boldsymbol{B} - \boldsymbol{B}\boldsymbol{V}) = 0 \quad (3)$$

$$\frac{\partial p}{\partial t} + \nabla \cdot (p\boldsymbol{V}) = -(\gamma - 1)p\nabla \cdot \boldsymbol{V} \quad (4)$$

where $\boldsymbol{f} = -\boldsymbol{\omega}\times[\boldsymbol{\omega}\times\boldsymbol{r} + \boldsymbol{2\omega}\times\boldsymbol{V}]$ is the additional force densities based on the coordinate transformation theory. The polytrophic index γ is taken as 1.46 in this study.

- The numerical scheme is based on the 3-D COIN-TVD MHD scheme [Feng et al., 2003, 2005; Shen et al., 2007, 2009].In this scheme, all of the physical quantities is computed from the conservation TVD Lax-Friedrich scheme in a Sun-centered spherical coordinate system.

How to deal with $\nabla \cdot \boldsymbol{B}$ Error

- The $\nabla \cdot \boldsymbol{B}$ error produced by the scheme is diffused away at the maximal rate allowed by iterating

$$\boldsymbol{B} \coloneqq \boldsymbol{B} + \mu(\Delta x)^2 \nabla \nabla \cdot \boldsymbol{B} \qquad (5)$$

where $(\Delta x)^2 = \frac{1}{\frac{1}{(\Delta r)^2}+\frac{1}{(r\Delta\theta)^2}+\frac{1}{(r\sin\theta\Delta\phi)^2}}$. For values of $\mu \in (0, 2)$, typically less than 10 iterations are sufficient to satisfy $\text{Max}\left(\frac{\iint B_n ds}{\iint |B_n| ds}\right) \leq 10^{-2}$.

Six-Component Mesh Grid System

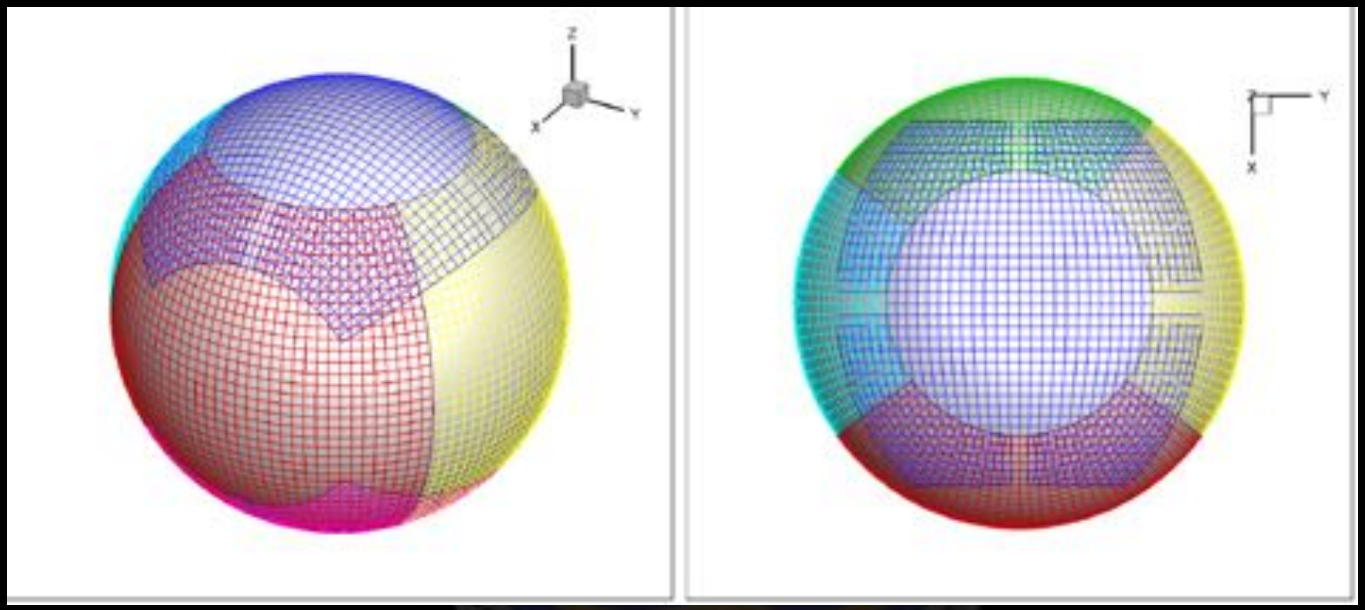

- To avoid the singularity in spherical coordinate system, six-component mesh grid system is used on the spherical shell [Feng, 2011].
- This grid system consists of six identical components meshes to envelope a spherical surface with partial overlap on their boundaries. Each component grid is a low-latitude spherical mesh, which is defined in the spherical coordinates;
- The computational domain covers $21.5R_s \leq r \leq 258R_s$, $-90° \leq \theta \leq 90°$, and $0° \leq \phi \leq 360°$
- The grid size gradually increases from $0.37R_s$ to $2.37R_s$ in r-direction, and in other directions, the grid resolution is $\Delta\phi = \Delta\theta = 1°$, corresponding with a time resolution of 1.8 hours

New boundary Treatment——B_r

- Firstly, we use the PFSS model to obtain the polarity of B_r by using GONG magnetogram as input;
- Although the PFSS model could be used to predict the IMF polarity quite well, it has a strong latitudinal variability and the field strength increases in magnitude away from the neutral line. We only keep the polarity of the B_r from the PFSS model and use the observational data at 1 AU to limit the value of B_r:

$$B_r = \mathrm{sign}\left(B^{\mathrm{PFSS}}\right) \times \frac{1}{\sqrt{2}} \mathrm{mean}\left(B^{1\mathrm{AU}}\right) \left(\frac{1\mathrm{AU}}{R_b}\right)^2 \qquad (6)$$

where $\mathrm{mean}\left(B^{1\mathrm{AU}}\right)$ is the average value of the observed magnetic field at 1AU from OMNI during the past three Carrington Rotations (CRs). Because of $\mathrm{mean}\left|B_\phi\right| \approx \mathrm{mean}|B_r|$ at 1 AU, B_0 is defined as $\frac{1}{\sqrt{2}}\mathrm{mean}\left(B^{1\mathrm{AU}}\right)$. After obtaining B_0, we can get the distribution of B_r at the lower boundary by considering the magnetic flux conservation and the polarity from the PFSS model .

New boundary Treatment——V_r

- The empirical WSA relation is used to assign solar wind speed:

$$V_r = V_s + \frac{V_f}{(1+f_s)^{a_1}}\left[1 - 0.8\exp\left(-\left(\frac{\theta_b}{a_2}\right)^{a_3}\right)\right]^{a_4} \qquad (7)$$

where V_s is the slowest speed, while V_f is the fastest speed, a_1-a_4 are free parameters. Both f_s and θ_b can be obtained from PFSS models.

- Here, we set V_f=675 km·s^{-1}, a_1=0.22, a_3=1.0， a_4=1.0, and keep two free parameters which are V_s and a_2.
- The number of multipole components included in the spherical harmonic expansion in PFSS models, L_{max}, can influence the distribution of f_s and θ_b to a good extent.
- We keep L_{max} as the primary regulatory factor and leave V_s and a_2 as the secondary regulatory parameters.

New boundary Treatment——*N*

- It is well known that there is a strong negative correlation between density and flow velocity, which implies that the density cannot be taken as a free parameter in solar wind models.
- The solar wind energy flux was found to be independent of solar wind speed and latitude, and this quantity varied weakly over the solar cycle [Chat et al., 2012, *Sol. Phys*.]. By setting the solar wind energy flux as a constant, the number density can be calculated by:

$$N = N_0 \left(\frac{1\mathrm{AU}}{R_b}\right)^2 V_0 \left(\frac{1}{2}V_0^2 + \frac{GM_s}{R_s}\right)\left[V_r\left(\frac{1}{2}V_r^2 + \frac{GM_s}{R_s}\right)\right]^{-1} \qquad (8)$$

Where N_0 and V_0 are the density and velocity at 1 AU. Set $V_0 = 750$ km/s, and N_0 can be deduced from the average solar wind energy flux during the past three CRs at 1 AU.

New boundary Treatment——T_p

- Here we choose to use the relation that the proton temperature is a quadratic function of the velocity at 1AU: $T_p \sim \frac{1}{2}V_r^2$, with T_p in Kelvin and V_r in km/s. Then we normalize T_p to $21.5R_s$ by the power law $T_p \sim \frac{1}{r^{2(\gamma-1)}}$:

$$T_p = \frac{1}{2}V_r^2 \times \left(\frac{1\text{AU}}{R_b}\right)^{2(\gamma-1)} \qquad (9)$$

New boundary Treatment——$V_\theta, V_\phi, B_\theta$ and B_ϕ

- When observed in the rest frame and supposing that the solar wind plasma flow propagates through the boundary in the radial direction, the meridional components V_θ and azimuthal flow velocity V_ϕ at the lower boundary in the co-rotation frame are determined by the follow formulas :

$$V_\theta = 0 \quad V_\phi = -\omega R_b \sin\theta \tag{10}$$

- When observed in the co-rotation frame, the magnetic field line would be parallel to the solar wind plasma flow at the steady state:

$$B_\theta = 0 \quad B_\phi = -\frac{\omega R_b \sin\theta}{V_r} B_r \tag{11}$$

Simulation Results——2007

CR2053 (from 4 February 2007 to 4 March 2007)

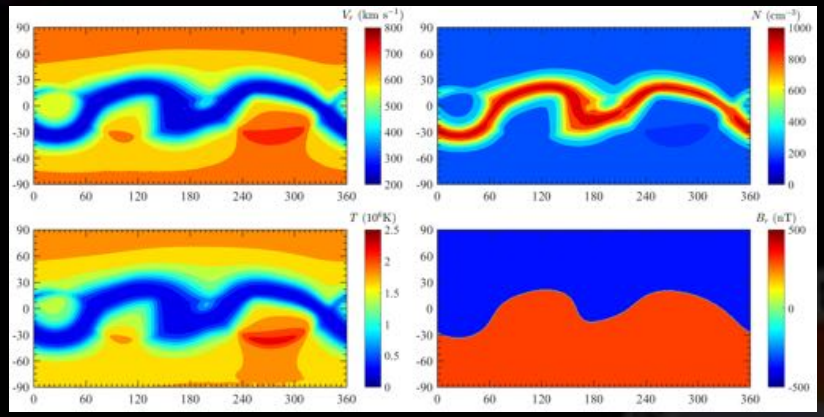

Distributions at the lower boundary

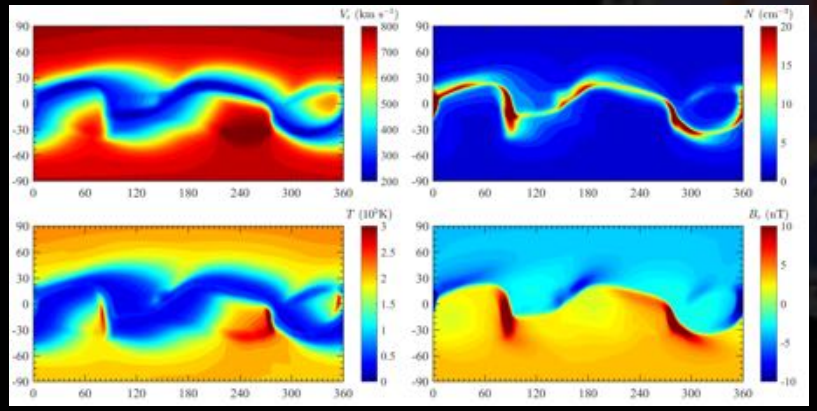

Distributions at 1AU

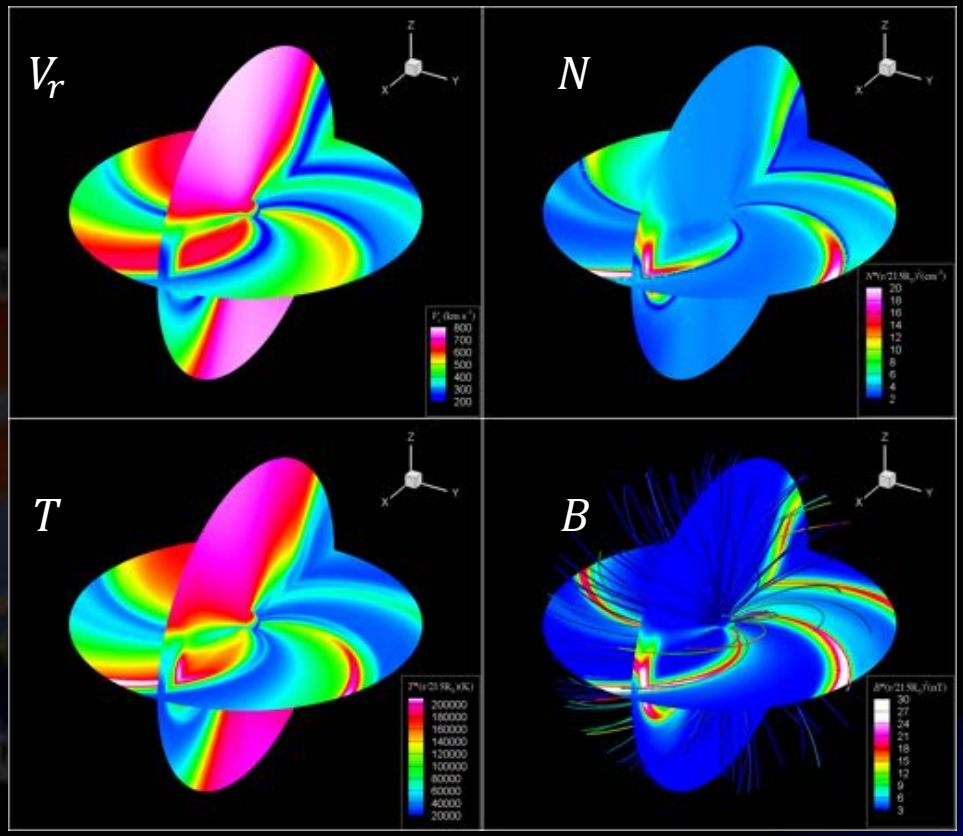

In the heliospheric equatorial and meridional plane

- At 1AU, there is a left shift of about 50° in longitudinal direction, which is a reflection of the corotating interaction effect. In low latitudes, a few compression regions and rarefaction regions are formed due to the interaction of the high speed streams (HSSs) and the low speed streams.
- The classic features of interplanetary solutions, that is, the high density CIRs between fast and slow solar wind streams, can be clearly recognized. Near the north pole and south pole, high speed wind is seen to dominate. However, there is a mix of slow and fast winds at all latitudes.

Validation of Simulation Result for Year 2007

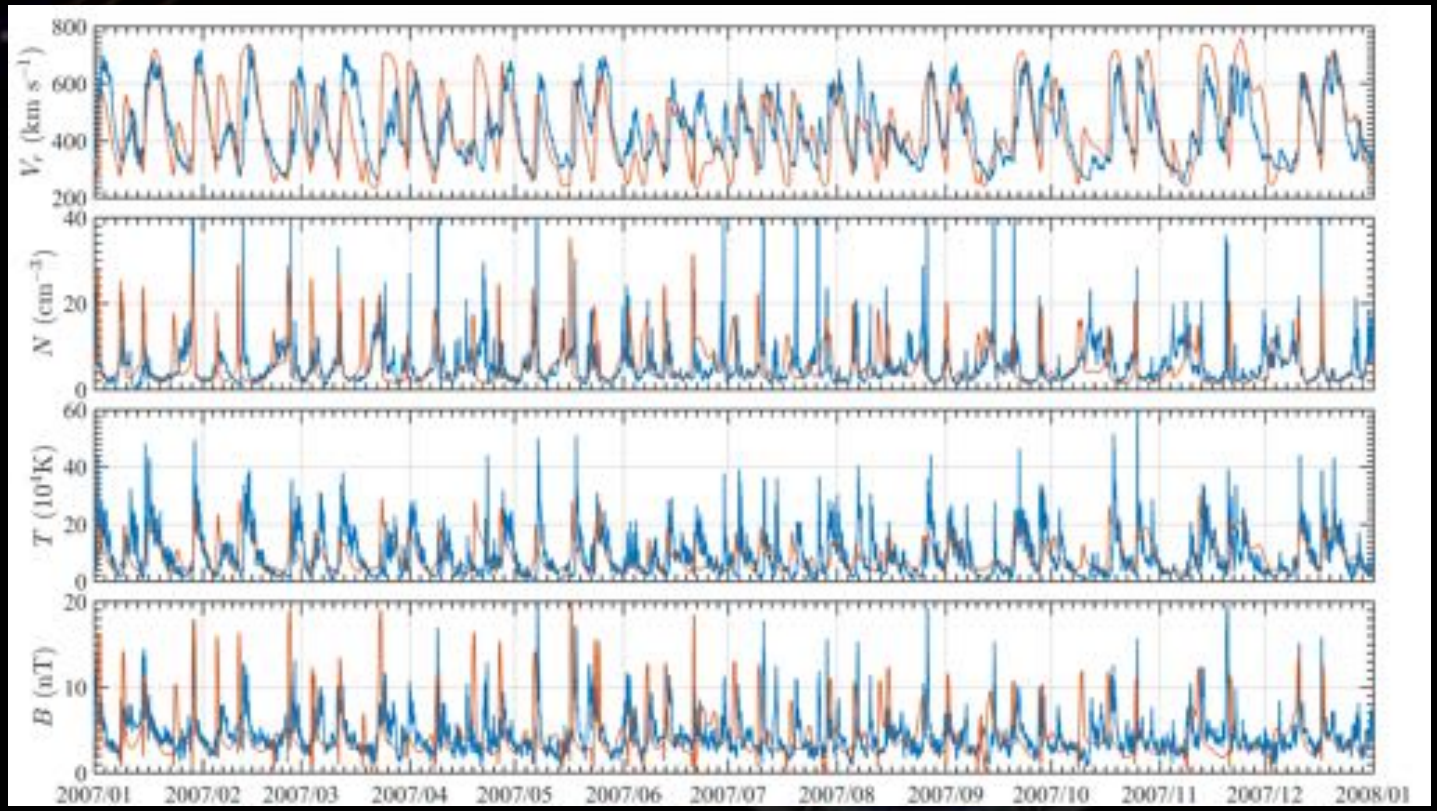

Modeled and observed profiles of solar wind parameters at 1AU

- Therefore, for the ambient solar wind, an accurate speed boundary condition is very important for predicting the magnetic field strength.

- The simulation can catch most of the HSSs. Moreover, the duration time and the magnitude of the HSSs are largely consistent with that of observations ;
- If the speed is well simulated, the density and the magnetic field strength fit the observations well, especially during the time intervals when the arrival times of HSSs coincide with that of the observations.

Validation of Simulation Result for Year 2007

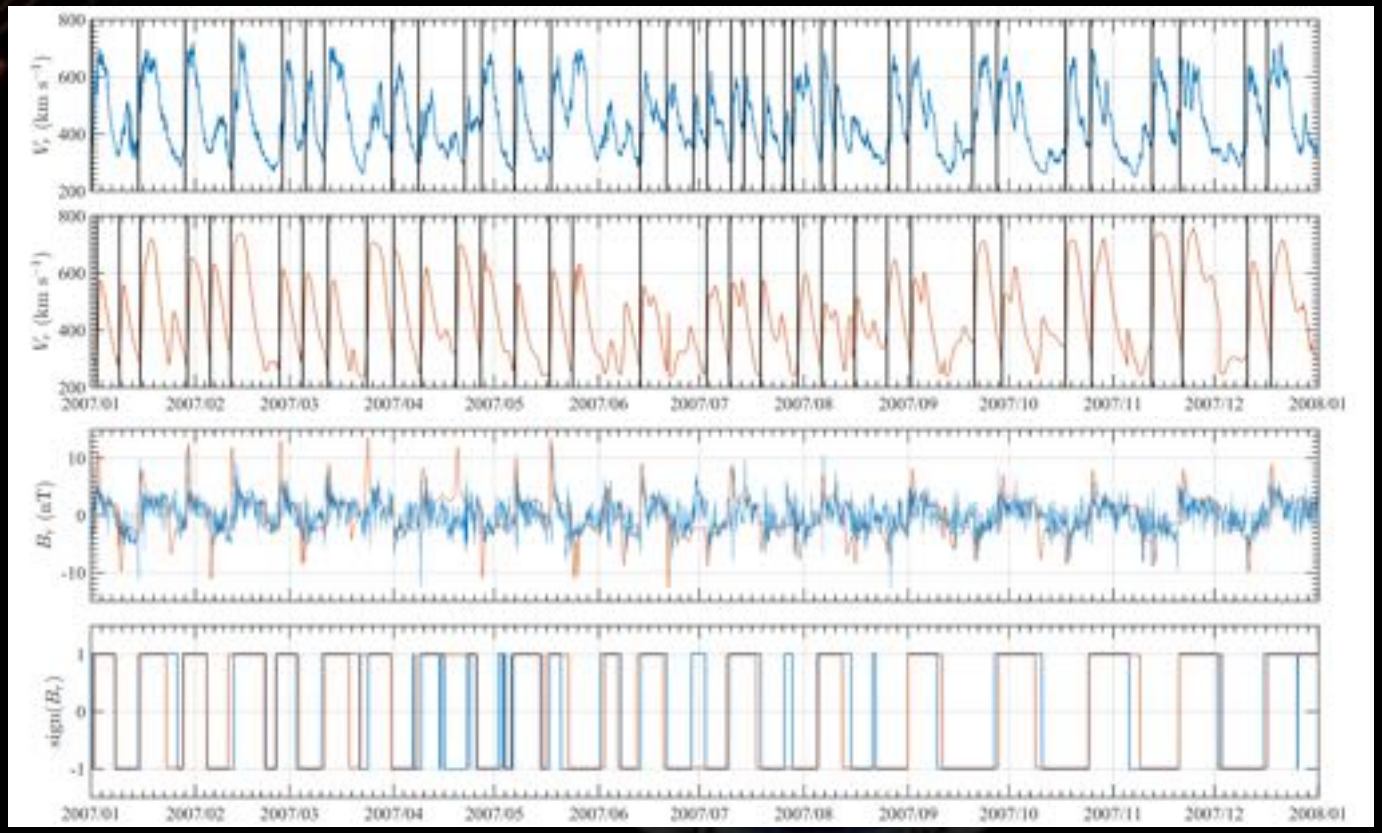

Observed and modeled high speed streams (HSSs)

Observed and modeled B_r at 1AU in 2007

$$\Delta t = t^M - t^O$$

Comparison of modeled and observed HSSs and in-ecliptic IMF polarity						
	hit	miss	hit rate	False alarm	Δt	$\lvert\Delta t\rvert$
HSSs	29	5	85%	15%	4±21hours	17±13hours
IMF polarity			~85%		-5±33hours	24±22hours

New boundary Treatment——Free Parameters

Ranges of free parameters at the lower boundary					
Parameters	L_{max}	V_s(km·s^{-1})	a_2(°)	N_0(cm^{-3})	B_0(nT)
Minimum	6	250	2.0	1.3	2.6
Maximum	15	300	4.0	2.7	5.3

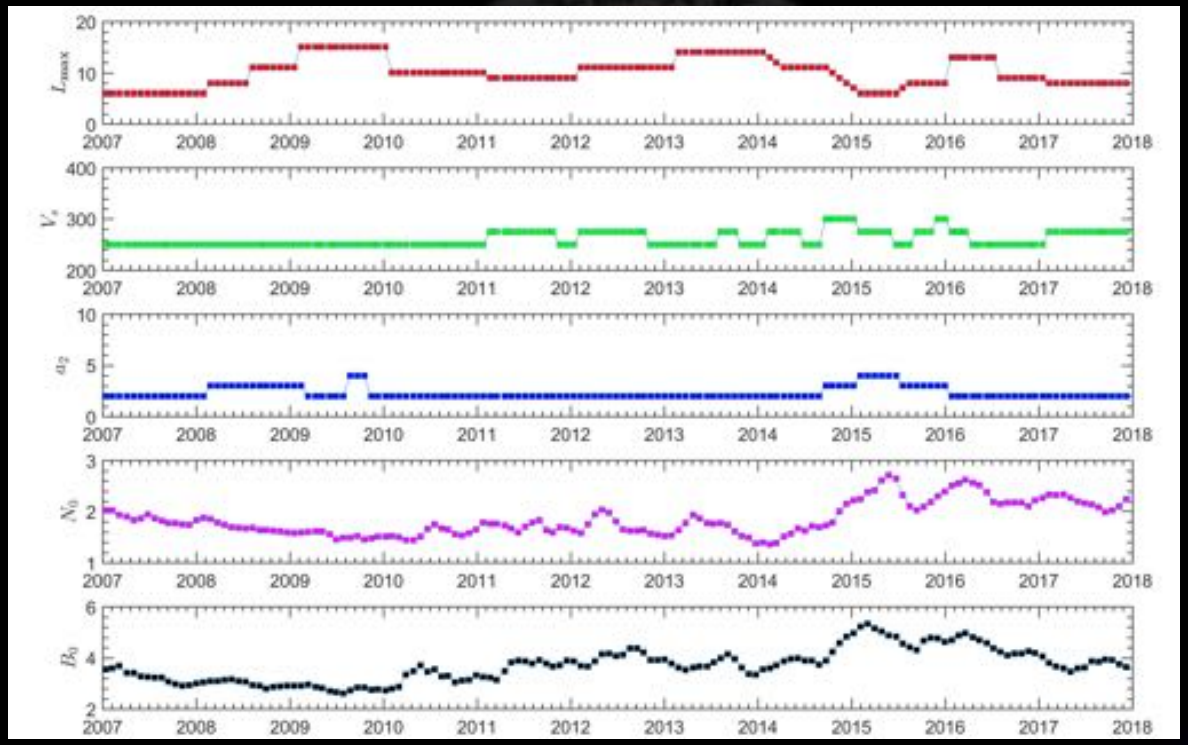

Value of the free parameters in boundary conditions from 2007 to 2017.

SIGMA WEATHER GROUP

Simulation Results——2008-2017

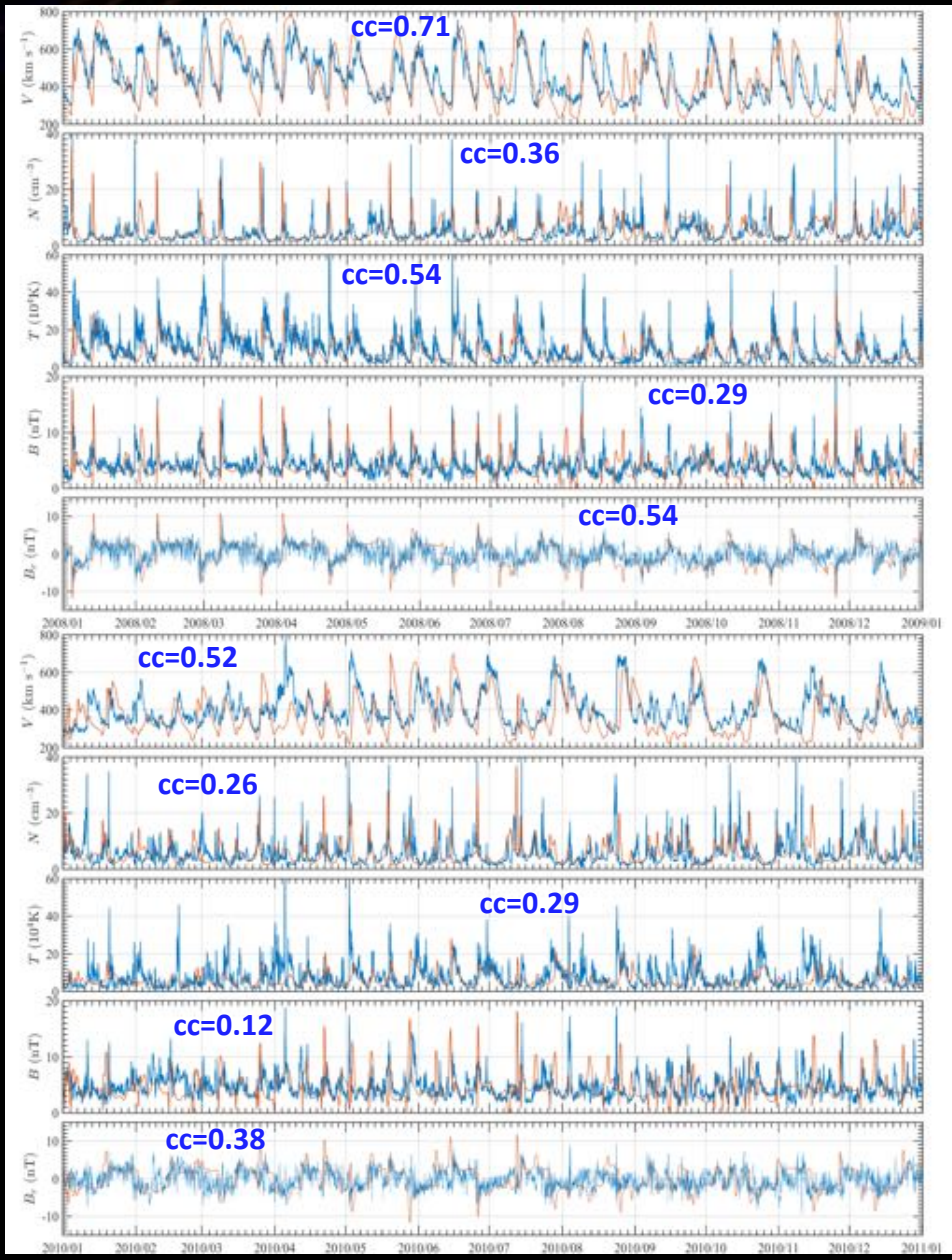

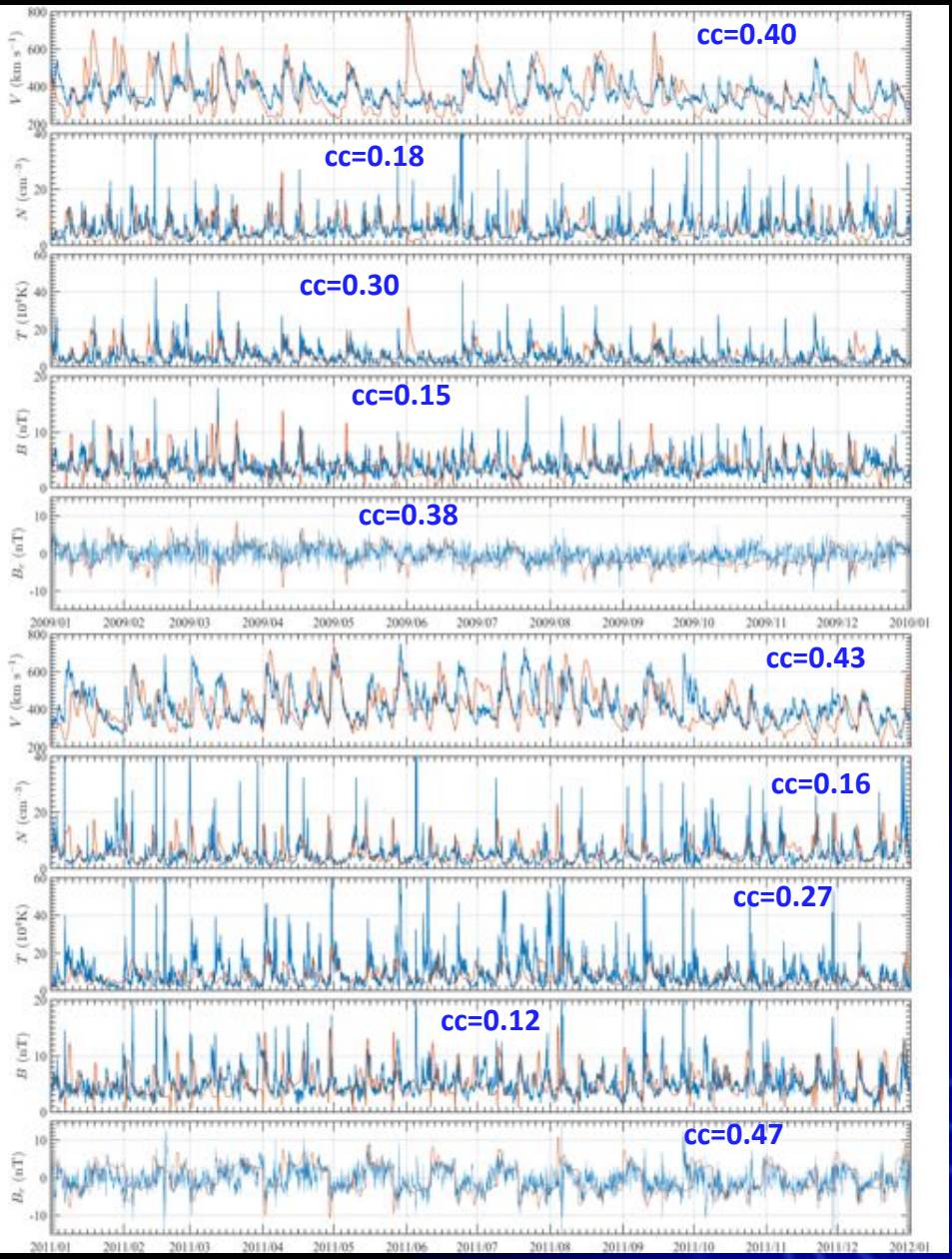

SIGMA WEATHER GROUP

Simulation Results——2008-2017

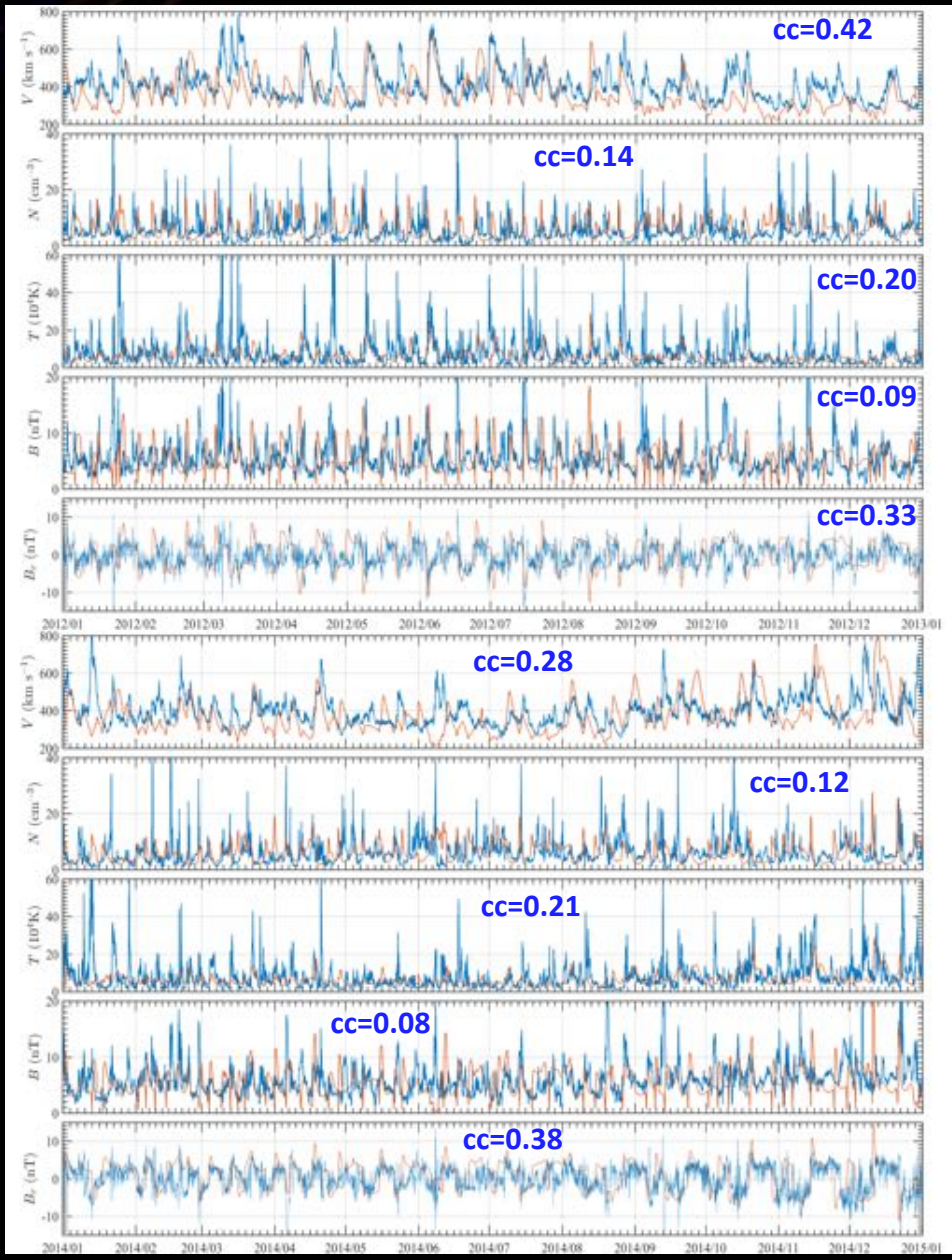

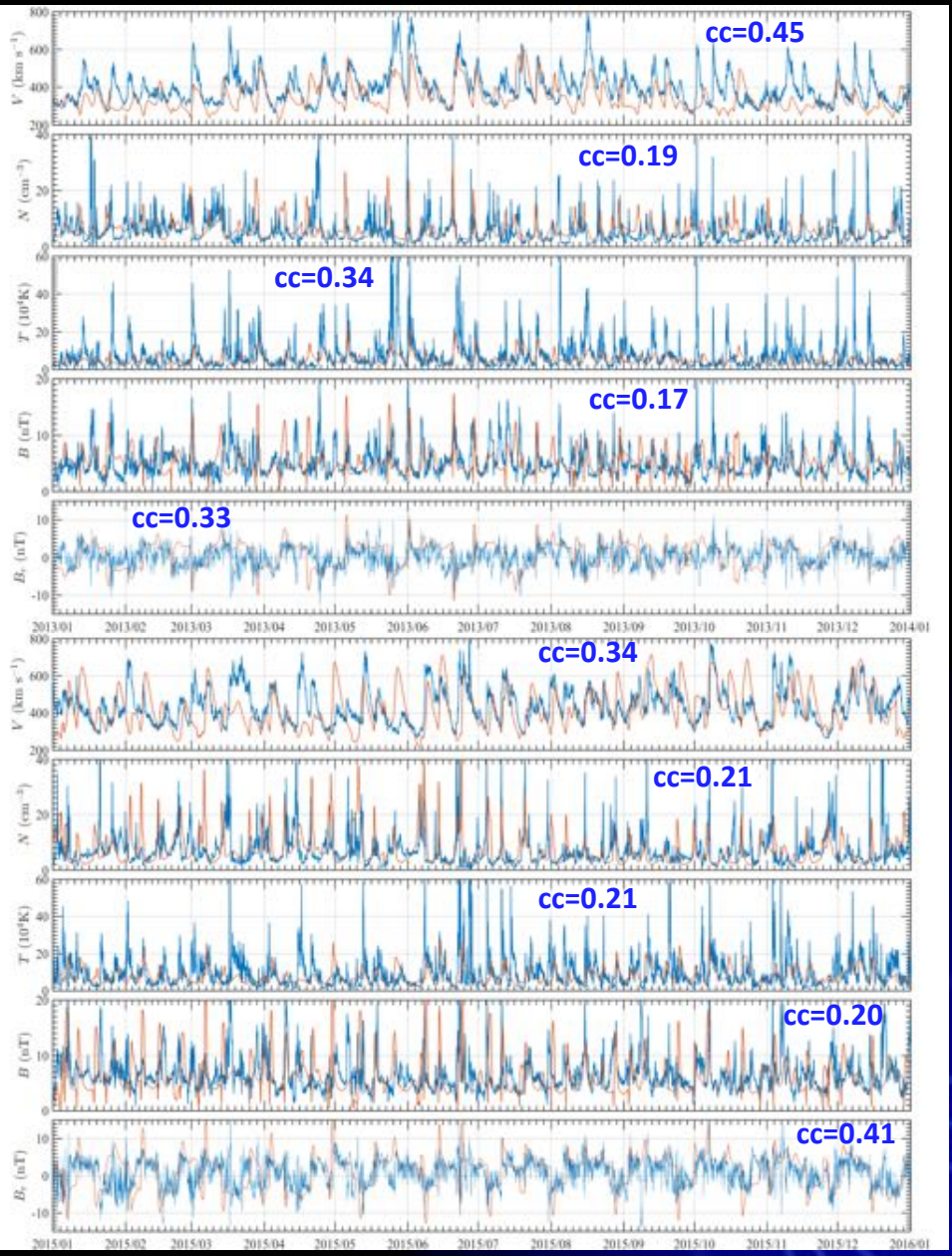

SIGMA WEATHER GROUP

Simulation Results——2008-2017

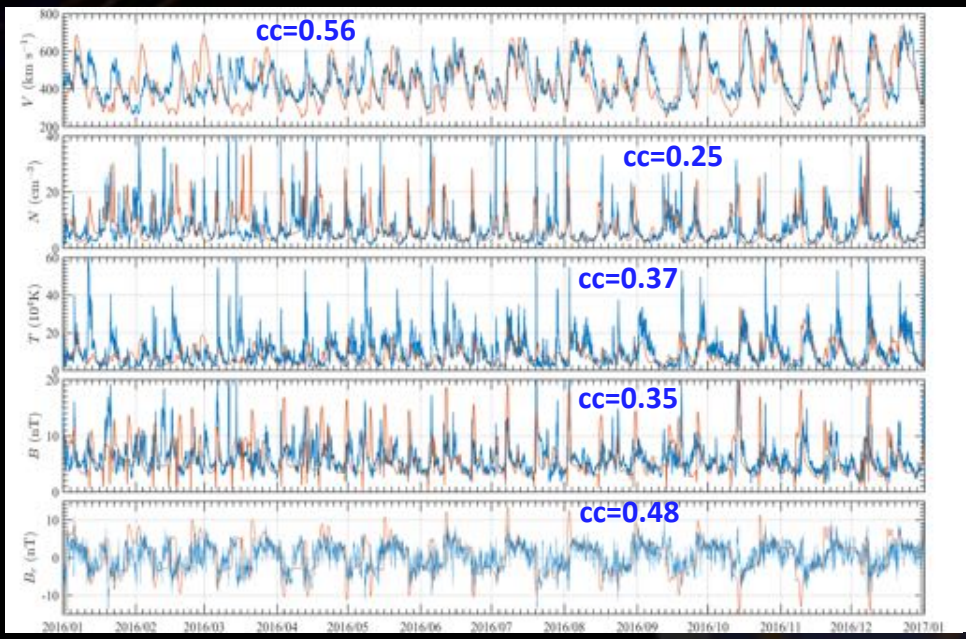

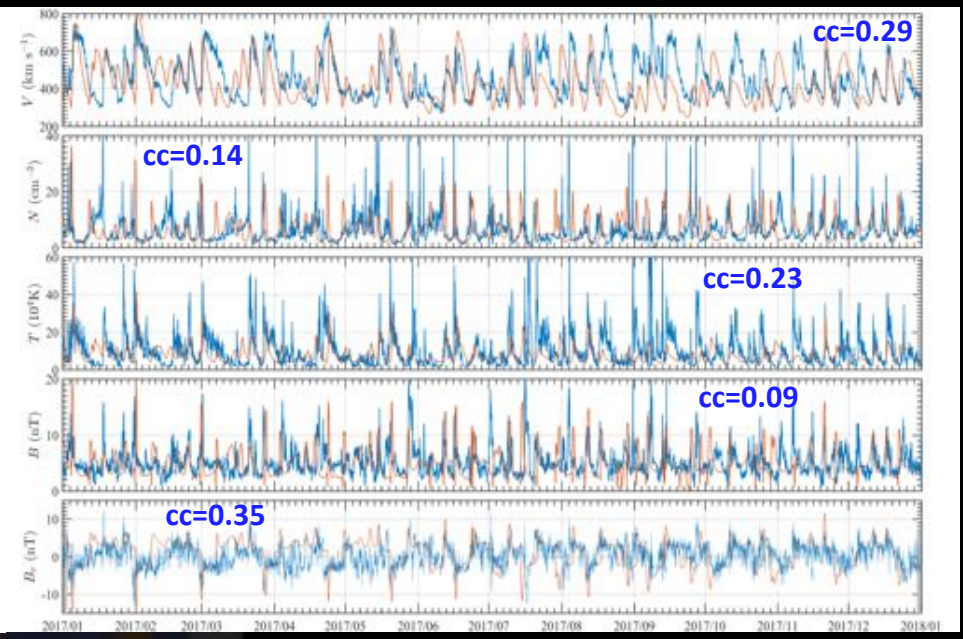

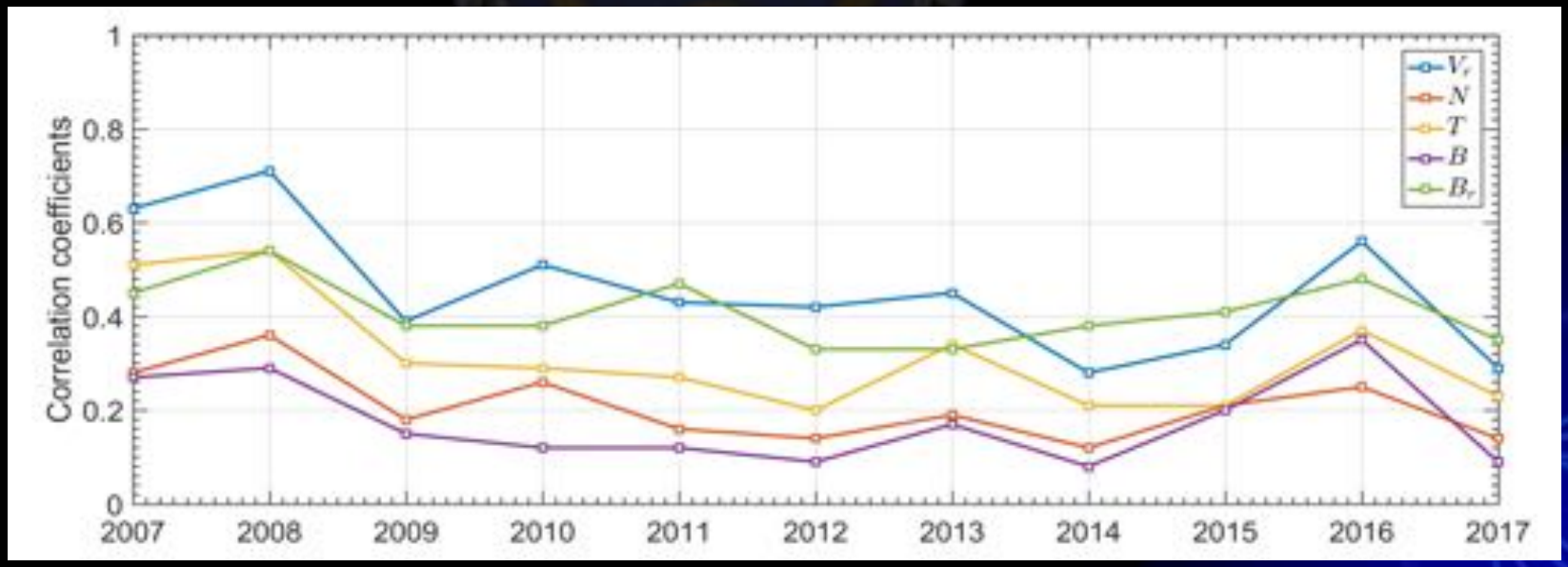

Discussion and Summary

- In this work, we employ an improved 3D IN-TVD MHD model with a new boundary treatment to simulate the propagation and distribution of the solar wind into the heliosphere;
- In the boundary conditions, we reserve five free parameters, so as to simulate the solar wind for different phases of solar cycle, and to improve the prediction of solar wind parameters;
- Using the improved MHD model with the new lower boundary conditions, we simulated the background solar wind from 2007 to 2017. Our simulation could reproduce most of the characteristic solar wind structures, e.g., HSSs, sector boundary as well as the amplitudes of solar wind parameters near the Earth, including *V*, *N*, *T*, *B* and B_r ;
- In our model, the parameters for tuning freely are very few and the ranges are also relative small. Further, based on the simulation of past 11 years, these parameters can maintain unchanged for quite long time (several CRs to several years). Therefore the improved IN-TVD model with the new boundary treatment can be applied for prediction/forecast of solar wind parameters near the Earth .

Shen, F., Z. Yang, J. Zhang et al. (2018), In press, *APJ*

Thanks